Neuron-derived Thioredoxin-80: a novel regulator of type-I interferon response in microglia

Julen Goikolea[1,#], Jean-Pierre Roussarie[2], Gorka Gerenu[3,4,5], Raul Loera-Valencia[1], Maria Latorre-Leal[1], Angel Cedazo-Minguez[1], Patricia Rodriguez-Rodriguez[1,*], Silvia Maioli[1,*].

[1]Department of Neurobiology, Care Sciences and Society, Division of Neurogeriatrics, Center for Alzheimer Research, Karolinska Institutet, Stockholm, Sweden.

[2]Boston University School of Medicine. Boston, Massachusetts. USA.

[3]Biodonostia Health Research Institute, Neuroscience Area, 20014, Donostia-San Sebastián, Gipuzkoa, Spain.

[4]CIBERNED (Network Center for Biomedical Research in Neurodegenerative Diseases), Carlos III Institute, Madrid, Spain.

[5]Department of Physiology, Medicine and Nursing School, University of Basque Country UPV/EHU, Leioa, Spain.

* These authors contributed equally to this work.

[#] Corresponding author: Julen Goikolea (julen.goicolea@ki.se)

Abstract

Oxidative stress and neuroinflammation play a central role in Alzheimer´s Disease (AD) pathogenesis. However, the mechanism by which these processes lead to neurodegeneration is still not fully understood. Thioredoxin-1 (Trx1) is an antioxidant protein that can be cleaved into a peptide known as Thioredoxin-80 (Trx80), which modulates monocyte function in the periphery and shows anti-amyloidogenic properties in the brain. In this study we aimed to further clarify the biological function of this peptide and its regulation in the brain. We show that neurons are the main producers of Trx80 in the brain. Trx80 levels increase *in vivo* both in normal aging and in young $APP^{NL\text{-}G\text{-}F}$ mouse model of amyloid pathology. Trx80 levels were increased in neurons in primary culture treated with either rotenone or 27-hydroxycholesterol, what suggests that Trx80 production is stimulated upon oxidative stress. RNA-sequencing followed by differential gene expression analysis revealed that Trx80 induces microglia activation into a phenotype compatible with interferon response microglia. Finally, we determine that the induction of this microglia phenotype by Trx80 is Trem2-dependent. This study identifies Trx80 as a novel neuron-derived signaling mechanism that modulates microglia function under stress conditions. Strategies to regulate Trx80 levels could be beneficial against AD pathology.

Keywords:

Microglia, Thioredoxin, Alzheimer´s Disease, Aging, Oxidative Stress, Inflammation

Abbreviations:

27-OHC, 27-hydroxycholesterol; Aβ, Amyloid-beta; AD, Alzheimer's Disease; Ank, Ankyrin1; ARM, Activated response microglia; bacTRAP, bacterial artificial chromosome – translating ribosome affinity purification; IRM, Interferon response microglia; Isg15, Interferon-stimulated gene 15; Ifit2, Interferon Induced Protein With Tetratricopeptide Repeats 2; Irf7, Interferon Regulatory Factor 7; Nrf2, Nuclear factor erythroid 2-related factor 2; Oasl2, 2'-5' oligoadenylate synthetase-like 2; Spp1, Secreted Phosphoprotein 1; Trem2, Triggering receptor expressed on myeloid cells 2; Trx1, Thioredoxin-1; Trx80, Thioredoxin-80.

46 **Introduction**

47 Microglia are the resident immune cells of the central nervous system and play important roles in
48 brain development and physiology (1). Their relevance in disease pathogenesis has gained
49 increasing interest in AD, where genome-wide association studies (GWAS) have established that
50 many AD genetic risk variants are confined to microglia transcriptional enhancer regions (2).
51 Moreover, rare genetic variants encoding triggering receptor expressed on myeloid cells 2
52 (TREM2), which plays an essential role as a regulator of microglia function, have been identified
53 as significant genetic risks factors for late onset AD (3-5). During AD pathology, a diversity of
54 microglial cell states has been identified (6-8). Of special interest are two different, mutually
55 exclusive, reactive microglia states present in normal aging that are modified by AD risk factors *in*
56 *vivo*: Activated Response Microglia (ARM) and Interferon Response Microglia (IRM)(9). ARMs
57 show overexpression of genes of the Major Histocompatibility complex type II (MHCII) and they are
58 enriched in AD risk genes whereas IRMs are characterized by an upregulation of type-I interferon
59 response genes. The mechanisms that govern the appearance of these different microglia states
60 and their role in neurodegeneration remain to be fully understood and could provide new avenues
61 for therapeutic intervention.

62 Thioredoxin-1 (Trx1) is a highly conserved endogenous dithiol with functions that span from
63 maintenance of cellular redox homeostasis to chemokine activity (10, 11). Trx1 can be cleaved into
64 an 80 amino acid long peptide, known as Thioredoxin-80 (Trx80) (12). Trx80 function has been
65 widely investigated in the periphery, where it is secreted and triggers innate immunity and pro-
66 inflammatory responses (13, 14).

67 Our group reported that Trx80 inhibits Aβ-induced toxic effects in cell cultures as well as Aβ42
68 accumulation in the brain (15). Moreover, Trx80 expression rescued the lifespan and locomotor
69 impairments observed in Aβ42-expressing *Drosophila melanogaster* models (16). Interestingly,
70 Trx80 protein levels are depleted in brains of AD patients (15). Nevertheless, the biological function
71 and mechanisms that regulate Trx80 production and secretion in the brain are still unknown.

72 In the present study we show that Trx80 levels in the brain are affected by aging and amyloid
73 pathology, two important drivers of AD pathology. Furthermore, we identify that oxidative stress, a
74 converging event for aging and amyloidosis increases Trx80 production by neurons. Finally, we
75 show that Trx80 leads to microglia differentiation into a type-I-interferon response transcriptional
76 profile in a Trem-2 dependent manner. Together, our results unveil a new mechanism that regulates
77 microglia function with implications for AD pathology.

78 **Materials and Methods**

79 ***Animals***

80 Male C57BL/6J wild-type mice at 2, 8 and 22 months of age were obtained from Janvier (Janvier
81 labs, Le Genest-Saint-Isle, France). Female 3 and 10 months old homozygous APP^{NL-G-F} knock in
82 mice and their wild-type C57BL/6J (WT) controls were available at our department at KI. Male 22
83 months old Cyp27A1 overexpressing mice and their littermate WT controls were available in our
84 group. Mice were kept under controlled temperature (21±1°C) and humidity (55±5%) on a 12-h
85 light-dark cycle and food/water were provided ad libitum.

86 ***Cortico-Hippocampal Mouse Primary Neurons and Microglia cultures***

87 Cortico-Hippocampal primary neuronal cultures from E17 C57BL/6J mouse embryos (Janvier labs)
88 were performed as previously reported (17). Briefly, dissected tissue was trypsinized in 0.25%
89 trypsin, 1mM EDTA (T4049, Merck, Darmstadt, Germany) in EBSS (#14155063, Thermo Fisher
90 Scientific, Waltham, Massachusetts, USA) for 15 minutes at 37°C. After centrifugation (500 x g,
91 5min) the tissue was mechanically disintegrated in a solution containing 170 ug/ml DNAse
92 (#10104159001, Merck) in EBSS. The supernatant was transferred to a fresh tube, centrifuged
93 (500 *x* g, 5 minutes) and the pellet was resuspended in serum-free neurobasal medium
94 (#21103049, Thermo Fisher Scientific) with B-27 (#17504044, Gibco, Thermo Fisher Scientific),
95 Penicillin/Streptomycin (#15140122, Thermo Fisher Scientific) and Glutamax (#35050061, Thermo
96 Fisher Scientific). Cultures were incubated at 37°C and 5 % CO_2.

97 Microglia and astrocyte cultures were performed following the procedure described for neurons,
98 but cells were resuspended in DMEM/F-12, GlutaMAX (#10565018, Thermo Fisher Scientific) and

99 supplemented with 10% Heat-inactivated FBS (#10500064, Gibco, Thermo Fisher Scientific) and
100 Penicillin/Streptomycin. Cultures were incubated at 37°C and 5 % CO_2 for 24h before complete
101 media change. Further media changes were performed every 3 days until confluency was reached.
102 Microglia was dissociated from mixed glial cultures by mild-trypsinization (0.25% trypsin, 1 mM
103 EDTA diluted 1:4 in DMEM/F-12, GlutaMAX serum-free) as previously reported (18).

104 ***Cell treatments***

105 All neuron treatments were performed at 10 days in vitro (DIV). Neurons were treated 1 μM 27-
106 hydroxycholesterol (27-OHC, Avanti Instruchemie, The Netherlands) or vehicle (DMSO, Sigma) for
107 2h before collection. 100 nM Rotenone (#R8875, Merck) or vehicle (DMSO) for 18h before
108 collection. 1 μM Trx80 (#2329-TX, R&D Systems, Minneapolis, Minnesota, USA) or vehicle (PBS)
109 for 24h before collection.

110 Microglia cultures were kept at 37°C and 5 % CO_2 for 24h before treatment. Cells were treated with
111 1 μM Trx80 peptide or vehicle (PBS) for 24h before collection.

112 ***Sample preparation and western blot***

113 Immunoblotting was performed as previously described (17). Briefly, mouse brain tissue and cell
114 lysates were homogenized in 50 mM Tris-HCL, 150 mM NaCl, 1% Triton-X containing phosphatase
115 and protease inhibitors (Sigma-Aldrich, St. Louis, Missouri, USA). Homogenates were run in
116 polyacrylamide gels (Bio-Rad, Hercules, California, USA and transferred to BioTraceTM
117 Nitrocellulose membranes (GE healthcare, Chicago, Illinois, USA). Membranes were blocked for
118 1h in 5% skim milk in TBS-Tween-20 (TBS-T) prior to overnight incubation with primary antibody
119 at 4°C. Primary antibodies: anti-Trx80 mouse (7D11 #11543, Cayman chemicals, Ann Arbor,
120 Michigan, USA), anti-Trx1 goat (#11538 Cayman chemicals), anti-NRF2 rabbit (ab137550, Abcam,
121 Cambridge, United Kingdom), Anti-β-Actin mouse (AC-15, Sigma-Aldrich), anti-GAPDH mouse
122 (6C5, ab8245, Abcam) and Anti-α-Tubulin antibody (T9026, Sigma-Aldrich). Fluorescent secondary
123 antibodies (LI-COR Biosciences, Lincoln, Nebraska, USA) were used for 2h at room temperature
124 and visualized using ODYSSEY Infrared Imaging System (LI-COR Biosciences). Band intensity

125 signal was quantified by ImageJ software. Each band signal value was normalized against loading
126 controls (tubulin/actin/GAPDH signal value).

127 ***RNA extraction and Real-time quantitative PCR***

128 Total RNA extraction, reverse transcription, and real-time quantitative PCR (RT-qPCR)
129 amplification was performed using the TaqMan Fast Advanced Cells-to-Ct Kit following the
130 manufacturer's instructions (Thermo Fisher). Briefly, cells were washed in PBS and lysed in
131 solution containing DNase for 5 minutes at room temperature. Lysis was terminated at room
132 temperature by a 2-minute incubation with Stop Solution. Lysates were reverse transcribed in a
133 SimpliAmp Thermal cycler (Life Technologies, Carlsbad, California, USA). Quantification of
134 selected genes was done using specific primers for *Ifit2, Ifit3, Irf7, Spp1, Axl, Trem2* and *Gapdh*
135 (Life Technologies) in a 7500 Fast Real-Time PCR system (Applied Biosystem, Life Technologies).
136 GAPDH was used as housekeeping gene.

137 ***Small Interference RNA Transfection***

138 *Trem2* and *Axl* knockdown were performed using siRNA designed by Horizon Discovery (Accell
139 Mouse Trem2 siRNA SMARTpool, E-040918-00-0005; Accell Mouse Axl siRNA SMARTpool, E-
140 040941-00-0005). Mouse primary microglia (80% confluence) were transfected with a final
141 concentration of 0.5 µM per well for 8h according to the manufacturer's instructions. The efficiency
142 of the knockdown were measured using mRNA levels of *Trem2* and *Axl*.

143 ***Immunofluorescence***

144 Microglial cells were fixed in 4% PFA for 10 min followed by permeabilization and washing steps
145 (0.25% Triton-X in PBS). Cells were then incubated in 5% BSA Blocking buffer 1 h at room
146 temperature. As primary antibodies, anti-Ifit2 rabbit (PA3-845, Sigma-Aldrich), anti-ISG15 rabbit
147 (PA5-79523, Thermo Fisher Scientific) anti-OPN goat (AF808-SP, R&D systems), anti-Iba-1 rabbit
148 (#019-19741, Wako, Japan) and anti-Iba-1 goat (NB100-1028, NOVUS) were incubated overnight
149 at 4°C. Thereafter, samples were washed three times and incubated 1h at room temperature with
150 secondary antibodies: Alexa Fluor Plus 488 goat anti-Rabbit (A32731, Thermo Fisher Scientific)

151 and Alexa Fluor Plus 546 donkey anti-goat (A11056, Thermo Fisher Scientific). Identification of the
152 nuclei of cell bodies was performed using 4, 6 diamino-2-phenylindole (DAPI; Sigma).

153 Immunofluorescence of mice cortical samples was performed as previously described (19). The
154 following primary antibodies were used: anti-Iba-1 goat and anti-Ifit2 rabbit. Sections were then
155 incubated for 2 h at room temperature with the secondary antibodies Alexa Fluor Plus 488 goat
156 anti-Rabbit and Alexa Fluor Plus 546 donkey anti-goat. Identification of the nuclei of cell bodies
157 was performed using DRAQ5 fluorescent prove solution (#62251, Thermo Fisher Scientific).
158 Omission of the primary antibody was done as a control staining. Sections were mounted using
159 fluorescence mounting medium (DAKO Cytomation, Glostrup, Denmark). Images were obtained in
160 a Zeiss LSM900-Airy confocal microscope performing a Z-stack at cortical areas. Fluorescence
161 intensity of Isg15 per microglial cell was measured by the ImageJ 1.383 software (NIH, MA, USA).

162 ***RNA sequencing***

163 Library preparation and RNA sequencing was outsourced to the Bioinformatics and Expression
164 Analysis (BEA) core facility at The Karolinska Institute. Briefly, total RNA was subjected to quality
165 control with Agilent Bioanalizer 2100 using an RNA pico chip according to the manufacturer's
166 instructions. cDNA libraries were prepared using the Truseq stranded mRNA samples preparation
167 protocol (Illumina, San Diego, California, USA), which includes mRNA isolation, cDNA synthesis,
168 ligation of adapters and amplification of indexed libraries. The yield and quality of the amplified
169 libraries was analyzed using Qubit (Thermo Fisher Scientific) and the Agilent TapeStation. Libraries
170 were then normalized, multiplexed and sequenced on the Illumina Nextseq 550 for a 75-cycle v2
171 sequencing run generating 75 bp single-end reads.

172 ***Statistical analysis***

173 All experiments were performed at least in triplicate. Statistical analysis was performed using
174 Prism software (GraphPad 9). Student's t-test was used to evaluate the significance of the
175 statistical difference between two groups. The statistical differences among three groups was
176 calculated using One-way analysis of variance (ANOVA). Fisher's exact test was used to assess

177 the gene expression overlap between Trx80-activated microglia, IRMs and ARMs. For all tests,
178 $P < 0.05$ was considered statistically significant.

179 **Results**

180 **Trx80 is produced by neurons and its levels are increased with normal aging and in young**
181 **Appki$^{NL\text{-}G\text{-}F}$ mouse**

182 The relative contribution of the different major cell types in the brain to the Trx80 pool is unknown.
183 To clarify this issue, we determined Trx80 protein levels in mouse primary cultures of neurons,
184 astrocytes, and microglia. Our results show that neurons display higher levels of Trx80 than
185 astrocytes and microglia ($p<0.005$ and $p<0.001$, respectively) (**Figure 1a**). These results agree with
186 previous reports that found most Trx80 immunoreactivity in pyramidal neurons in the human brain
187 (15). Protein levels of its precursor Trx1, were, however, comparable between these cell types. RT-
188 qPCR analysis revealed that *Txn1* (the gene that codes for Trx1) expression is higher in neurons
189 than in astrocytes or microglia ($p<0.0001$) (**Figure 1b**). These results are in agreement with publicly
190 available *in vivo* single-cell transcriptomics data (**Figure 1c**, Allen Institute for Brain Science (2020),
191 celltypes.brain-map.org/rnaseq (20)). Together, these data suggests that, as opposed to the other
192 cell types, a big proportion of Trx1 in neurons is transformed into Trx80.

193 To investigate the effect of amyloid pathology on Trx80 levels in the brain, we used APP$^{NL\text{-}G\text{-}F}$
194 knock-in mice. This mouse model exhibits early amyloidosis and reactive gliosis at 2-3 months of
195 age (21). We measured Trx80 protein levels in cortical samples from 3-month old (n=5 WT, n=5
196 APP$^{NL\text{-}G\text{-}F}$) and 10-month old (n=4 WT, n=5 APP$^{NL\text{-}G\text{-}F}$) female mice by western blot. Our results
197 show that Trx80 is increased in 3-month old APP$^{NL\text{-}G\text{-}F}$ mice compared to wild-type controls
198 ($p<0.0001$, **Figure 1c**). However, Trx80 levels were decreased ($p<0.05$) compared to controls in
199 10-month old APP$^{NL\text{-}G\text{-}F}$ mice (**Figure 1d**) resembling the decrease previously described in human
200 AD brains (15).

201 To test whether aging, the most significant non-genetic risk factor for late-onset AD (22) affects
202 Trx80 levels in the brain, we analyzed Trx1 and Trx80 protein levels in 2, 8 and 22 months old wild-
203 type (WT) male mice. Western blot analysis of cortical homogenates did not show significant

204 changes in Trx1 or Trx80 levels between 2 and 8 months of age. At 22 months, Trx1 levels
205 decreased, while Trx80 levels increased compared to 2- and 8-month old mice ($p>0,05$, $p<0.01$
206 respectively, **Figure 1e**). While Trx80 increases 1.7-fold between 8- and 22-months of age, Trx1
207 decreases 0.5-fold, what suggests additional mechanisms, other than cleavage of the precursor,
208 that specifically upregulate Trx80 at the protein level.

209 To further clarify *Txn1* expression levels in different brain regions and its changes during the mouse
210 lifespan in a cell-specific manner, we revisited publicly available neuron-specific bacTRAP-RNAseq
211 data from 5-, 12- and 24-month-old wild type mice (alz.princeton.edu) (23). As shown in **Figure 1f**,
212 *Txn1* gene expression is higher in neurons of AD-relevant and memory-associated brain regions,
213 such as principal neurons of the layer II of the entorhinal cortex (ECII neurons, the first neurons to
214 degenerate in AD) and CA1, CA2 and CA3 pyramidal neurons in the hippocampal formation,
215 compared to pyramidal neurons of the primary somatosensory cortex and granule neurons of the
216 dentate gyrus. *Txn1* expression is significantly decreased in ECII neurons between 5 and 24
217 months of age (log FC = -0.47, FDR = 0.036) (23).

218 **Oxidative stress induces Trx80 production by neurons**

219 Considering that Trx80 is the cleavage product of the antioxidant Trx1, we hypothesized that
220 oxidative stress, a common event in aging and early amyloid pathology, might modulate Trx80
221 production. To test this hypothesis, we treated neuronal primary cultures with rotenone, a known
222 inducer of oxidative damage (24-26). As expected, western blot analysis of neurons treated with
223 100 nM rotenone for 18h showed increased levels of nuclear factor erythroid 2-related factor
224 2 (NRF2), a well-known redox homeostasis regulator (27) (**Figure 2a**). Trx1 is a transcriptional
225 target of Nrf2 (28), and its levels, together with Trx80 were increased in rotenone-treated neurons
226 compared to control ($p<0.0001$, $p<0.001$ and $p<0.05$, respectively, **Figure 2a**).

227 To study this mechanism in more physiological conditions and *in vivo* we used the cholesterol
228 metabolite 27-hydroxycholesterol (27-OHC). 27-OHC is a cholesterol metabolite that is elevated in
229 AD brains (29) and causes oxidative stress (30, 31). We determined the effects of 27-OHC by
230 profiling neurons 2h after 1μM 27-OHC treatment using RNA-sequencing. As expected, differential

231 gene expression analysis (DGE) showed that 27-OHC modulates genes involved in cholesterol
232 metabolism (**supplementary figure 1a** and **1b**) and pathway analysis revealed alterations in Nrf2-
233 mediated oxidative response, among others (**supplementary figure 1c)**. Western blot analysis
234 showed that Nrf2, Trx1 and Trx80 protein levels were increased in 27-OHC treated neurons
235 compared to vehicle-treated controls ($p<0.05$, $p<0.01$ and $p<0.01$, respectively**, Figure 2b**). We
236 next analyzed Trx80 levels in brain homogenates from a 27-OHC overproducing (Cyp27Tg)
237 transgenic mouse model. These mice overexpresses the enzyme Cyp27A1, that converts
238 cholesterol into 27-OHC, and hence have higher 27-OHC levels than wild-type controls (32) (33).
239 Western blot analysis of Trx80 protein levels in cortical samples from 22 months old Cyp27Tg male
240 mice (n=7) and age and sex-matched wild-type littermates (n=8) showed increased Trx80 levels in
241 Cyp27Tg animals compared to controls ($p<0.001$, **Figure 2c**).

242 **Trx80 induces an interferon type-I response in microglia in a Trem2-dependent manner**

243 To study whether Trx80 modulates microglial function, we treated mouse microglia in primary
244 culture with 1μM recombinant Trx80 for 24h. RNA-sequencing followed by DGE analysis between
245 Trx80 and vehicle-treated microglia revealed *Hpgd* as one of the most significantly downregulated
246 genes in Trx80-treated microglia (**Figure 3a and 3b**). *Hpgd* codifies for 15-hydroxyprostaglandin
247 dehydrogenase that participates in prostaglandins degradation and thus in the regulation of
248 inflammatory response (34). Indeed, pathway analysis showed neuroinflammation and activation
249 of interferon regulatory factors by cytosolic pattern recognition receptors as some of the top
250 significantly upregulated pathways in Trx80-treated microglia, supporting the notion that Trx80
251 triggers a proinflammatory response in these cells (**Figure 3c**).

252 To clarify whether Trx80 induces a reactive microglia phenotype, we compared the differentially
253 expressed genes in Trx80-activated microglia with the gene signatures of ARMs and IRMs (9). The
254 transcriptional profile of Trx80-activated microglia showed a highly significant overlap only with
255 IRMs (**Figure 3d, 3e**). Specifically, we observed an increase in genes defined as IRM markers by
256 previous studies (30), such as *Ifit2*, *Ifit3*, *Irf7* and *Oasl2*, as well as an increase in other interferon
257 response-related genes (e.g. *Ifit1* and *Isg15*). *Igf1*, *Spp1* and *Ank*, described as upregulated

258 markers of ARMs, where found to be decreased in Trx80-treated microglia compared to control
259 (**Figure 3f**). *Ifit2*, *Ifit3*, *Irf7* and *Spp1* gene expression changes were confirmed in Trx80-treated
260 microglia by RT-qPCR analysis in an independent experiment ($p<0.05$, $p<0.001$, $p<0.0001$ and
261 $p<0.001$, respectively **supplementary Figure 2a**). This effect was not seen in Trx80-treated
262 neurons (**supplementary Figure 2b**). Immunofluorescence staining of Ifit2, ISG15 and osteopontin
263 (OPN, Spp1 protein) on Trx80 and vehicle-treated microglia showed higher Ifit2 and ISG15 protein
264 levels ($p<0.0001$) and decreased Spp1 levels Trx80-activated microglia compared to control
265 ($p<0.001$) (**Figure 4a, b and c**). Immunofluorescence analysis of ISG15 in 22 months old Cyp27Tg
266 mice showed higher ISG15-positive microglia than age-matched wild-type controls ($p<0.0001$)
267 (**Figure 4d**).

268 We finally aimed to determine the molecular mechanism regulating Trx80-induced IRM phenotype.
269 Trem2 is a transmembrane receptor that plays an essential role in microglia activation (3, 4) and
270 its genetic variants have been associated with AD (5). Axl receptor tyrosine kinase is another
271 transmembrane receptor that is upregulated in AD and described as a modulator of microglia-
272 mediated phagocytosis of Aβ plaques (35) and pro-inflammatory signaling (36). To test whether
273 the induction of an IRM phenotype in microglia by Trx80 is mediated by Trem2 or Axl, we knocked
274 down each of these genes in mouse microglia in primary culture, followed by Trx80 treatment
275 (**Figure 5a**). RT-qPCR analysis showed that partial Trem2 knock down prevents the Trx80-
276 mediated increase in *Ifit2*, *Ifit3* and *Irf7* gene expression while it doesn't affect *Spp1* gene
277 downregulation. Knocking down Axl did not trigger significant differences in Trx80-induced
278 expression of *Ifit2*, *Ifit3* and *Irf7* compared to control (scrambled shRNA transfected) microglia
279 (**Figure 5b**). These results suggest that Trx80 effect on microglia interferon-response is Trem2-
280 dependent.

281 **Discussion**

282 Trx80 peptide is found in the brain (15), where it prevents Aβ aggregation and inhibits Aβ toxic
283 effects (15, 16). Despite its role on Aβ clearing, its biological function in the brain remains to be
284 fully understood. Indeed, most of the studies on Trx80 have been performed in peripheral blood

285 mononuclear cells, where it acts as a pro-inflammatory cytokine for monocytes, inducing their
286 replication and enhancing the recruitment of lymphocytes (12-14). Innate immune pathways and
287 neuroinflammation play an essential role in the pathogenesis of AD (37, 38). Therefore, in the
288 present study we aimed to investigate the mechanisms regulating Trx80 synthesis in the brain, how
289 they are affected by aging and AD-relevant pathological contexts and the effect of Trx80 on
290 microglia function.

291 Trx1, Trx80 precursor, shows similar protein levels in all cell types: neurons, astrocytes and
292 microglia. However, Trx1 mRNA levels were higher in neurons as well as Trx80 protein levels,
293 pointing at neurons as the main source of Trx80 in the brain. These results suggest that neurons
294 dedicate a part of Trx1 expression for Trx80 production under basal conditions. A previous study
295 identified the metalloproteases ADAM10/17 as responsible for Trx1 cleavage into Trx80 (15). Our
296 results suggest that the activity or the levels of these enzymes might be higher in neurons than in
297 other cell types of the brain. This notion is supported by a previous study showing that ADAM10
298 levels are higher in neurons than in astrocytes (39).

299 We next analyzed Trx80 levels on $APP^{NL\text{-}G\text{-}F}$ mouse brain homogenates, observing higher Trx80
300 levels at 3 months, followed by a decrease at 10 months of age. Interestingly, increased levels of
301 Trx80 take place at the same age as the first Aβ depositions occur in this mouse model (21). This
302 suggests that Trx80 production increases as an early stress response to Aβ accumulation, Aβ
303 oligomers-induced alterations on neurons or secondary to inflammation induced by oligomers.
304 Indeed, previous studies suggested that Trx80 is an early danger-response signaling molecule in
305 the periphery (14). An explanation for its decrease at 10 months is that at this age, $APP^{NL\text{-}G\text{-}F}$ mice
306 show widespread Aβ depositions, prominent gliosis and synaptic loss, which could be translated
307 into alterations in neuronal function, and possibly in the levels and/or activities of the
308 metalloproteases responsible for the cleavage of its precursor (21, 40).

309 By analyzing cortical homogenates from wild-type mice at different ages, we showed that Trx80
310 levels increase with age, while Trx1 levels decrease over time. These results agree with previous
311 studies of Trx1 and Trx80 levels on blood serum samples in a population of young and older adults

312 (41). Trx1 levels decrease progressively throughout the mouse lifespan, while Trx80 increase after
313 8 months of age. These results support the notion that Trx80 levels are not only a consequence of
314 the abundance of its precursor, but that they are regulated in a specific manner, most likely by the
315 activity of the enzymes responsible for Trx1 cleavage (41) or its degradation.

316 Oxidative stress is a key factor in the cellular effects caused by aging (42-44). Elevated Aβ levels
317 have been associated with oxidized byproducts of proteins, lipids, and nucleic acids in AD brains
318 and *in vitro* Aβ treatments elevate intracellular ROS levels in neurons (45, 46). Therefore, we
319 hypothesized that both aging and Aβ pathology could lead to increased Trx80 levels due to
320 oxidative stress. Furthermore, alterations in the levels of cholesterol metabolites have been
321 associated with AD (47) and 27-OHC, a cholesterol metabolite that is elevated in AD brains (29),
322 leads to oxidative stress (30, 31). Here we show that both rotenone (*in vitro*) and 27-OHC (*in vitro*
323 and *in vivo*) induce Nrf2 signaling and increased Trx80 levels in neurons. Interestingly, the cleavage
324 of Trx1 into Trx80 renders the peptide devoid of its redox capacity (48). This, together with our
325 results suggests that neurons increase Trx80 production under stress conditions with other
326 purposes than mere antioxidant defense.

327 We next investigated the effects of Trx80 on microglia. Expression analysis on Trx80-treated
328 microglia revealed that most upregulated pathways are associated with inflammatory response and
329 processes related to viral and bacterial recognition and elimination. This transcriptional profile
330 matches the effects of Trx80 reported in the periphery (14). Importantly, the transcriptional profile
331 of Trx80-activated microglia shows significant similarities to the IRM subset of reactive microglia
332 (9). The role of IRMs in the brain is still unknown. However, DNA damage promotes the production
333 of type-I interferons (49) and IRMs have been found in the proximity to neurons harboring DNA
334 damage (50), amyloid plaques containing nucleic acids (51), and to be enriched with age in the
335 human brain (52). Altogether, these studies suggest that IRMs are associated with basal
336 surveillance of neuronal stress and overall neuronal damage present in aging-related processes.
337 Our results showing that Trx80 increases in the brain with age, suggest that Trx80 could be involved
338 in the appearance of IRMs in aged brains. A microglia subset that is enriched in interferon response
339 genes has recently been found in MCI and AD brains (8). Our results, showing an early increase

340 in Trx80 in a mouse model of amyloid pathology, supports an association of this axis with AD
341 pathology, however, whether the presence of interferon response microglia promotes or hinders
342 the development of AD remains unknown.

343 DAMs phenotype induction was previously shown to take place in two sequential steps: a Trem2-
344 independent step, followed by a Trem2-dependent step (6). The mechanisms driving other
345 phenotypes such as IRMs are still unknown. Here we provide evidence that Trx80 induces an IRM-
346 like phenotype, and that this response is also dependent on Trem2. This finding suggests that IRMs
347 and DAMs (9), although distinct and independent microglia phenotypes, are driven by Trem2 in
348 combination with other signaling mechanisms that differ depending on the specific trigger and the
349 biological context.

350 **Conclusions**

351 Our findings identify Trx80 as a novel neuronal stress-induced signaling peptide that regulates
352 microglia function. However, further work needs to be done to elucidate the potential contribution
353 of Trx80 to the appearance of IRMs in different contexts and to fully understand the role of this
354 microglia phenotype in health and disease.

355 **Availability of data and materials**

356 The datasets used and/or analyzed during the current study are available from the corresponding
357 author on reasonable request.

358 **Conflict of interests**

359 All authors declare that there were no conflicts of interests.

360 **Authors' contributions**

361 J.G., P.R. and S.M. designed the study. J.G. acquired and collected the *in vitro* and *in vivo* data
362 with the help of R.L.V., G.G. and M.L.. P.R., JP.R. analyzed the RNA-sequencing data. J.G. wrote
363 the manuscript. A.C.M., P.R. and S.M revised the manuscript. All authors read, commented and
364 approved the final manuscript.

365 **Acknowledgments**

366 We would like to thank the Bioinformatics and Expression Analysis (BEA) core facility for their
367 service and help with the RNA-sequencing analysis and Biomedicum Imaging Core (BIC) facility at
368 Karolinska Institutet for their service with microscopy imaging.

369 **Ethics Approval**

370 All procedures involving animals were approved by the local ethical committee in Stockholm
371 (Ethical approval number: 4884/2019).

372 **Funding**

373 This research was supported by the Margaretha af Ugglas Foundation, the Karolinska Institutet
374 KID funding, Gun och Bertil Stohnes Stiftelse, Stiftelsen Syskonen Svenssons, the Karolinska
375 Institutet fund for geriatric research Stiftelsen Gamla Tjänarinnor and the regional agreement on
376 medical training and clinical research (ALF) between Stockholm County Council and Karolinska
377 Institutet.

378 **REFERENCES**

379 1. Hemonnot AL, Hua J, Ulmann L, Hirbec H. Microglia in Alzheimer Disease: Well-Known
380 Targets and New Opportunities. Front Aging Neurosci. 2019;11:233.
381 2. Nott A, Holtman IR, Coufal NG, Schlachetzki JCM, Yu M, Hu R, et al. Brain cell type-
382 specific enhancer-promoter interactome maps and disease-risk association. Science.
383 2019;366(6469):1134-9.
384 3. Kober DL, Brett TJ. TREM2-Ligand Interactions in Health and Disease. Journal of
385 molecular biology. 2017;429(11):1607-29.
386 4. Nugent AA, Lin K, van Lengerich B, Lianoglou S, Przybyla L, Davis SS, et al. TREM2
387 Regulates Microglial Cholesterol Metabolism upon Chronic Phagocytic Challenge. Neuron.
388 2020;105(5):837-54 e9.
389 5. Ulland TK, Song WM, Huang SC, Ulrich JD, Sergushichev A, Beatty WL, et al. TREM2
390 Maintains Microglial Metabolic Fitness in Alzheimer's Disease. Cell. 2017;170(4):649-63 e13.
391 6. Keren-Shaul H, Spinrad A, Weiner A, Matcovitch-Natan O, Dvir-Szternfeld R, Ulland TK,
392 et al. A Unique Microglia Type Associated with Restricting Development of Alzheimer's Disease.
393 Cell. 2017;169(7):1276-90 e17.
394 7. Krasemann S, Madore C, Cialic R, Baufeld C, Calcagno N, El Fatimy R, et al. The
395 TREM2-APOE Pathway Drives the Transcriptional Phenotype of Dysfunctional Microglia in
396 Neurodegenerative Diseases. Immunity. 2017;47(3):566-81 e9.
397 8. Olah M, Menon V, Habib N, Taga MF, Ma Y, Yung CJ, et al. Single cell RNA sequencing
398 of human microglia uncovers a subset associated with Alzheimer's disease. Nat Commun.
399 2020;11(1):6129.
400 9. Sala Frigerio C, Wolfs L, Fattorelli N, Thrupp N, Voytyuk I, Schmidt I, et al. The Major
401 Risk Factors for Alzheimer's Disease: Age, Sex, and Genes Modulate the Microglia Response to
402 Abeta Plaques. Cell Rep. 2019;27(4):1293-306 e6.
403 10. Arner ES, Holmgren A. Physiological functions of thioredoxin and thioredoxin reductase.
404 Eur J Biochem. 2000;267(20):6102-9.

11. Lovell MA, Xie C, Gabbita SP, Markesbery WR. Decreased thioredoxin and increased thioredoxin reductase levels in Alzheimer's disease brain. Free Radic Biol Med. 2000;28(3):418-27.
12. Pekkari K, Avila-Carino J, Bengtsson A, Gurunath R, Scheynius A, Holmgren A. Truncated thioredoxin (Trx80) induces production of interleukin-12 and enhances CD14 expression in human monocytes. Blood. 2001;97(10):3184-90.
13. Cortes-Bratti X, Basseres E, Herrera-Rodriguez F, Botero-Kleiven S, Coppotelli G, Andersen JB, et al. Thioredoxin 80-activated-monocytes (TAMs) inhibit the replication of intracellular pathogens. PLoS One. 2011;6(2):e16960.
14. Pekkari K, Goodarzi MT, Scheynius A, Holmgren A, Avila-Carino J. Truncated thioredoxin (Trx80) induces differentiation of human CD14+ monocytes into a novel cell type (TAMs) via activation of the MAP kinases p38, ERK, and JNK. Blood. 2005;105(4):1598-605.
15. Gil-Bea F, Akterin S, Persson T, Mateos L, Sandebring A, Avila-Carino J, et al. Thioredoxin-80 is a product of alpha-secretase cleavage that inhibits amyloid-beta aggregation and is decreased in Alzheimer's disease brain. EMBO Mol Med. 2012;4(10):1097-111.
16. Gerenu G, Persson T, Goikolea J, Calvo-Garrido J, Loera-Valencia R, Pottmeier P, et al. Thioredoxin-80 protects against amyloid-beta pathology through autophagic-lysosomal pathway regulation. Mol Psychiatry. 2021;26(4):1410-23.
17. Rodriguez-Rodriguez P, Sandebring-Matton A, Merino-Serrais P, Parrado-Fernandez C, Rabano A, Winblad B, et al. Tau hyperphosphorylation induces oligomeric insulin accumulation and insulin resistance in neurons. Brain. 2017;140(12):3269-85.
18. Saura J, Tusell JM, Serratosa J. High-yield isolation of murine microglia by mild trypsinization. Glia. 2003;44(3):183-9.
19. Merino-Serrais P, Loera-Valencia R, Rodriguez-Rodriguez P, Parrado-Fernandez C, Ismail MA, Maioli S, et al. 27-Hydroxycholesterol Induces Aberrant Morphology and Synaptic Dysfunction in Hippocampal Neurons. Cereb Cortex. 2019;29(1):429-46.
20. Yao Z, van Velthoven CTJ, Nguyen TN, Goldy J, Sedeno-Cortes AE, Baftizadeh F, et al. A taxonomy of transcriptomic cell types across the isocortex and hippocampal formation. Cell. 2021;184(12):3222-41 e26.
21. Saito T, Matsuba Y, Mihira N, Takano J, Nilsson P, Itohara S, et al. Single App knock-in mouse models of Alzheimer's disease. Nat Neurosci. 2014;17(5):661-3.
22. Wyss-Coray T. Ageing, neurodegeneration and brain rejuvenation. Nature. 2016;539(7628):180-6.
23. Roussarie JP, Yao V, Rodriguez-Rodriguez P, Oughtred R, Rust J, Plautz Z, et al. Selective Neuronal Vulnerability in Alzheimer's Disease: A Network-Based Analysis. Neuron. 2020;107(5):821-35 e12.
24. Mohammed F, Gorla M, Bisoyi V, Tammineni P, Sepuri NBV. Rotenone-induced reactive oxygen species signal the recruitment of STAT3 to mitochondria. FEBS Lett. 2020;594(9):1403-12.
25. Zhou Q, Liu C, Liu W, Zhang H, Zhang R, Liu J, et al. Rotenone induction of hydrogen peroxide inhibits mTOR-mediated S6K1 and 4E-BP1/eIF4E pathways, leading to neuronal apoptosis. Toxicological sciences : an official journal of the Society of Toxicology. 2015;143(1):81-96.
26. Zagoura D, Canovas-Jorda D, Pistollato F, Bremer-Hoffmann S, Bal-Price A. Evaluation of the rotenone-induced activation of the Nrf2 pathway in a neuronal model derived from human induced pluripotent stem cells. Neurochemistry international. 2017;106:62-73.
27. Yamamoto M, Kensler TW, Motohashi H. The KEAP1-NRF2 System: a Thiol-Based Sensor-Effector Apparatus for Maintaining Redox Homeostasis. Physiol Rev. 2018;98(3):1169-203.
28. Jakobs P, Serbulea V, Leitinger N, Eckers A, Haendeler J. Nuclear Factor (Erythroid-Derived 2)-Like 2 and Thioredoxin-1 in Atherosclerosis and Ischemia/Reperfusion Injury in the Heart. Antioxid Redox Signal. 2017;26(12):630-44.
29. Testa G, Staurenghi E, Zerbinati C, Gargiulo S, Iuliano L, Giaccone G, et al. Changes in brain oxysterols at different stages of Alzheimer's disease: Their involvement in neuroinflammation. Redox Biol. 2016;10:24-33.

460 30. Dasari B, Prasanthi JR, Marwarha G, Singh BB, Ghribi O. The oxysterol 27-
461 hydroxycholesterol increases beta-amyloid and oxidative stress in retinal pigment epithelial cells.
462 BMC Ophthalmol. 2010;10:22.
463 31. Ma WW, Li CQ, Yu HL, Zhang DD, Xi YD, Han J, et al. The oxysterol 27-
464 hydroxycholesterol increases oxidative stress and regulate Nrf2 signaling pathway in astrocyte
465 cells. Neurochem Res. 2015;40(4):758-66.
466 32. Meir K, Kitsberg D, Alkalay I, Szafer F, Rosen H, Shpitzen S, et al. Human sterol 27-
467 hydroxylase (CYP27) overexpressor transgenic mouse model. Evidence against 27-
468 hydroxycholesterol as a critical regulator of cholesterol homeostasis. The Journal of biological
469 chemistry. 2002;277(37):34036-41.
470 33. Ismail MA, Mateos L, Maioli S, Merino-Serrais P, Ali Z, Lodeiro M, et al. 27-
471 Hydroxycholesterol impairs neuronal glucose uptake through an IRAP/GLUT4 system
472 dysregulation. J Exp Med. 2017;214(3):699-717.
473 34. Kim HJ, Lee S, Lee HY, Won H, Chang SH, Nah SS. 15-hydroxyprostaglandin
474 dehydrogenase is upregulated by hydroxychloroquine in rheumatoid arthritis fibroblast-like
475 synoviocytes. Mol Med Rep. 2015;12(3):4141-8.
476 35. Huang Y, Happonen KE, Burrola PG, O'Connor C, Hah N, Huang L, et al. Microglia use
477 TAM receptors to detect and engulf amyloid beta plaques. Nature immunology. 2021;22(5):586-
478 94.
479 36. Gilchrist SE, Goudarzi S, Hafizi S. Gas6 Inhibits Toll-Like Receptor-Mediated
480 Inflammatory Pathways in Mouse Microglia via Axl and Mer. Front Cell Neurosci.
481 2020;14:576650.
482 37. Salter MW, Stevens B. Microglia emerge as central players in brain disease. Nature
483 medicine. 2017;23(9):1018-27.
484 38. Simon E, Obst J, Gomez-Nicola D. The Evolving Dialogue of Microglia and Neurons in
485 Alzheimer's Disease: Microglia as Necessary Transducers of Pathology. Neuroscience.
486 2019;405:24-34.
487 39. Guo ZB, Su YY, Wang YH, Wang W, Guo DZ. The expression pattern of Adam10 in the
488 central nervous system of adult mice: Detection by in situ hybridization combined with
489 immunohistochemistry staining. Mol Med Rep. 2016;14(3):2038-44.
490 40. Marcello E, Musardo S, Vandermeulen L, Pelucchi S, Gardoni F, Santo N, et al. Amyloid-
491 beta Oligomers Regulate ADAM10 Synaptic Localization Through Aberrant Plasticity
492 Phenomena. Mol Neurobiol. 2019;56(10):7136-43.
493 41. Couchie D, Vaisman B, Abderrazak A, Mahmood DFD, Hamza MM, Canesi F, et al.
494 Human Plasma Thioredoxin-80 Increases With Age and in ApoE(-/-) Mice Induces Inflammation,
495 Angiogenesis, and Atherosclerosis. Circulation. 2017;136(5):464-75.
496 42. Chen X, Guo C, Kong J. Oxidative stress in neurodegenerative diseases. Neural
497 regeneration research. 2012;7(5):376-85.
498 43. Luo J, Mills K, le Cessie S, Noordam R, van Heemst D. Ageing, age-related diseases and
499 oxidative stress: What to do next? Ageing Res Rev. 2020;57:100982.
500 44. Tan BL, Norhaizan ME, Liew WP, Sulaiman Rahman H. Antioxidant and Oxidative
501 Stress: A Mutual Interplay in Age-Related Diseases. Front Pharmacol. 2018;9:1162.
502 45. Varadarajan S, Kanski J, Aksenova M, Lauderback C, Butterfield DA. Different
503 mechanisms of oxidative stress and neurotoxicity for Alzheimer's A beta(1--42) and A beta(25--
504 35). Journal of the American Chemical Society. 2001;123(24):5625-31.
505 46. Yatin SM, Aksenova M, Aksenov M, Markesbery WR, Aulick T, Butterfield DA. Temporal
506 relations among amyloid beta-peptide-induced free-radical oxidative stress, neuronal toxicity, and
507 neuronal defensive responses. J Mol Neurosci. 1998;11(3):183-97.
508 47. Staurenghi E, Cerrato V, Gamba P, Testa G, Giannelli S, Leoni V, et al. Oxysterols
509 present in Alzheimer's disease brain induce synaptotoxicity by activating astrocytes: A major role
510 for lipocalin-2. Redox Biol. 2021;39:101837.
511 48. Pekkari K, Avila-Carino J, Gurunath R, Bengtsson A, Scheynius A, Holmgren A.
512 Truncated thioredoxin (Trx80) exerts unique mitogenic cytokine effects via a mechanism
513 independent of thiol oxido-reductase activity. FEBS Lett. 2003;539(1-3):143-8.

514 49. Hartlova A, Erttmann SF, Raffi FA, Schmalz AM, Resch U, Anugula S, et al. DNA
515 damage primes the type I interferon system via the cytosolic DNA sensor STING to promote anti-
516 microbial innate immunity. Immunity. 2015;42(2):332-43.
517 50. Mathys H, Adaikkan C, Gao F, Young JZ, Manet E, Hemberg M, et al. Temporal Tracking
518 of Microglia Activation in Neurodegeneration at Single-Cell Resolution. Cell Rep. 2017;21(2):366-
519 80.
520 51. Roy ER, Wang B, Wan YW, Chiu G, Cole A, Yin Z, et al. Type I interferon response
521 drives neuroinflammation and synapse loss in Alzheimer disease. The Journal of clinical
522 investigation. 2020;130(4):1912-30.
523 52. Olah M, Patrick E, Villani AC, Xu J, White CC, Ryan KJ, et al. A transcriptomic atlas of
524 aged human microglia. Nat Commun. 2018;9(1):539.
525

526

527 **Figure 1**

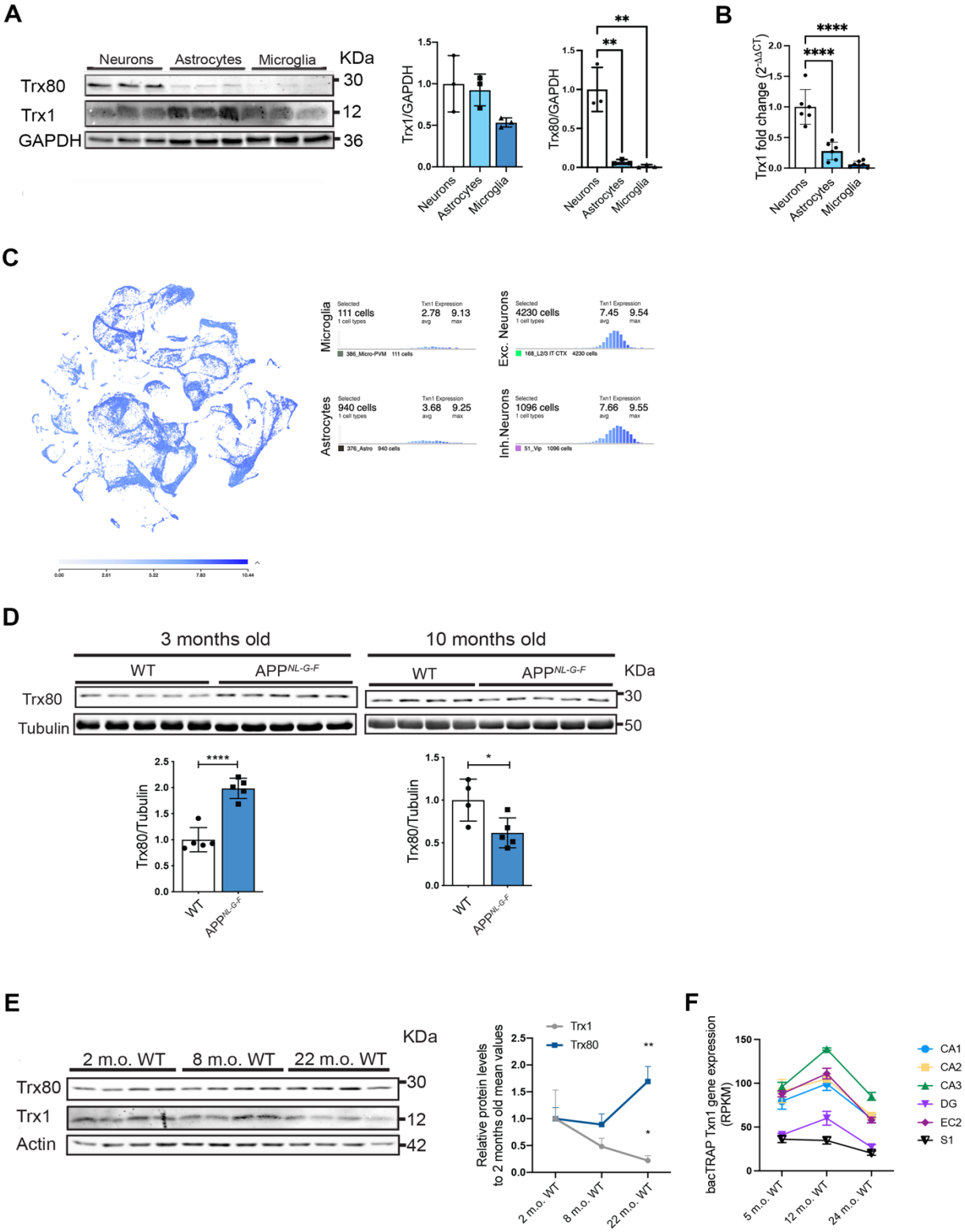
A
Neurons
Astrocytes
Microglia
KDa
Trx80
Trx1
GAPDH
30
12
36
Trx1/GAPDH
Trx80/GAPDH
B
Trx1 fold change (2-ΔΔCT)
C
Microglia
Exc. Neurons
Astrocytes
Inh.Neurons
D
3 months old
10 months old
WT
APPNL-G-F
Tubulin
50
Trx80/Tubulin
E
2 m.o. WT
8 m.o. WT
22 m.o. WT
Actin
42
Relative protein levels to 2 months old mean values
F
bacTRAP Txn1 gene expression (RPKM)
5 m.o. WT
12 m.o. WT
24 m.o. WT
CA1
CA2
CA3
DG
EC2
S1

528 **Figure 1. Trx80 is produced by neurons and its levels are increased with normal ageing and**
529 **in young Appki$^{NL\text{-}G\text{-}F}$ mouse model of amyloid pathology. A)** Western-blot analysis of mouse
530 primary neurons, astrocytes and microglia. Trx80, Trx1, GFAP and Iba-1 band intensities are
531 normalized against GAPDH (n=3 biological replicates). Results are expressed as mean ± SD. **B)**
532 RT-qPCR analysis of Txn1 gene expression levels in mouse primary neurons, astrocytes and
533 microglia. Values were normalized against each samples *Gapdh* gene expression levels. **C)** *Txn1*
534 gene expression from *in vivo* single-cell transcriptomics data Allen brain map transcriptomics
535 explorer. **D)** Western-blot quantification of Trx80 protein levels in 3- and 10- month old wild-type
536 and App$^{NL\text{-}G\text{-}F}$ mice cortical homogenates (3-month old, n=5 wild-type, n=5 App$^{NL\text{-}G\text{-}F}$; 10-month old,
537 n=4 wild-type, n=5 App$^{NL\text{-}G\text{-}F}$). Band intensities were normalized against tubulin. **E)** Western-blot
538 quantification of Trx80 and Trx1 in 2-, 8- and 22-month old wild-type mice cortical homogenates
539 (n=4 mice per group). Trx80 and Trx1 band intensities were normalized against actin. **F**) *Txn1* gene
540 expression in neuron-specific bacTRAP-RNAseq data from different brain regions at 5-, 12- and
541 24-month old wild type mice. Brain regions include the layer II of the entorhinal cortex (EC2),
542 hippocampal CA1, CA2 and CA3, somatosensory cortex (S1) and the dentate gyrus (DG).
543 Statistical analysis between groups in the 2-, 8- and 22-month old wild-type mice brains was
544 performed by one-way ANOVA for each protein. Statistical analysis between App$^{NL\text{-}G\text{-}F}$ and wild-
545 type mice was performed by Student t-test (*p<0.5; **p<0.01; ***p<0.001; **** p<0.0001).

546

547 **Figure 2**

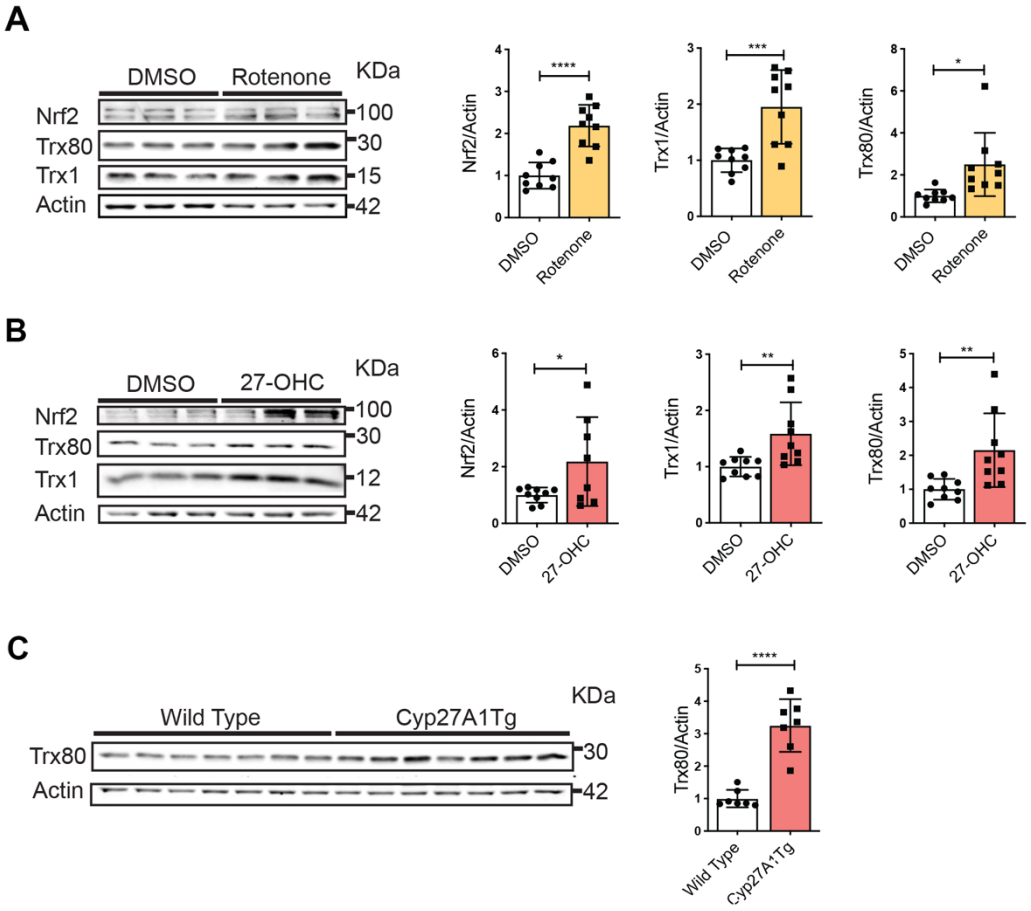

548
549 **Figure 2. Rotenone and 27-hydroxycholesterol treatment induce an increased production of**
550 **Trx80 in neurons. A)** Western-blot analysis of neuronal primary cultures treated with 100 nM
551 rotenone for 18h. Trx80, Trx1 and Nrf2 band intensities are normalized against Actin (n=3 biological
552 replicates). **B)** Western-blot analysis of neuronal primary cultures treated with 1 μM 27-
553 hydroxycholesterol for 2h. Trx80, Trx1 and Nrf2 are normalized against Actin (n=3 biological
554 replicates). **C)** Western-blot quantification of Trx80 in 22-month old wild-type and Cyp27A1
555 overexpressing mice cortical homogenates (n=7 wild-type, n=7 Cyp27A1Tg). Results are shown
556 as relative to controls. Statistical analysis was performed by Student t-test (*p<0.5; **p<0.01;
557 ***p<0.001; **** p<0.0001).
558
559
560
561
562
563

564 **Figure 3**

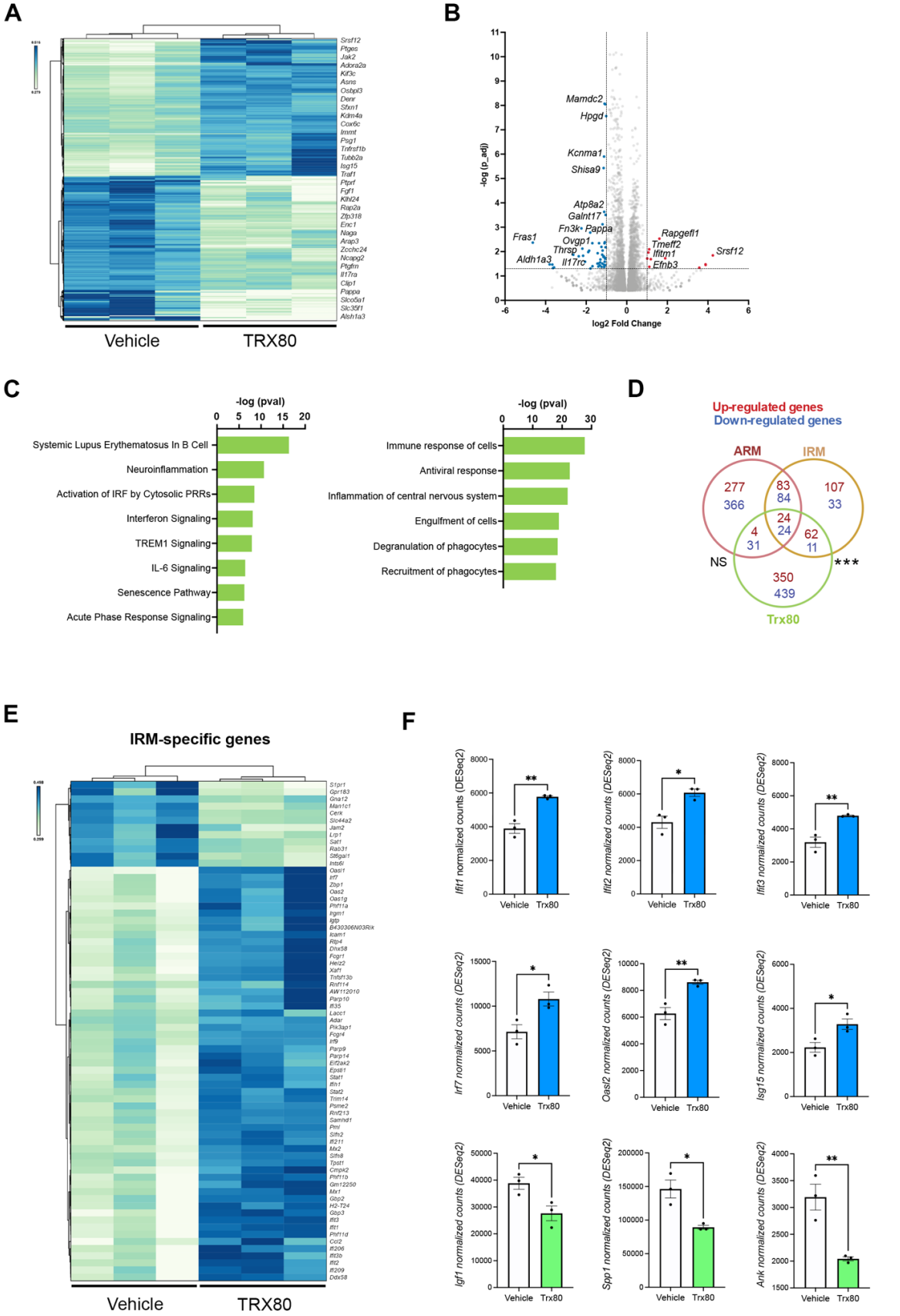
A
Vehicle
TRX80
B
-log (p_adj)
log2 Fold Change
Mamdc2
Hpgd
Kcnma1
Shisa9
Atp8a2
Galnt17
Fn3k
Pappa
Fras1
Ovgp1
Thrsp
Aldh1a3
Il17rc
Rapgefl1
Tmeff2
Ifitm1
Efnb3
Srsf12
C
-log (pval)
Systemic Lupus Erythematosus In B Cell
Neuroinflammation
Activation of IRF by Cytosolic PRRs
Interferon Signaling
TREM1 Signaling
IL-6 Signaling
Senescence Pathway
Acute Phase Response Signaling
Immune response of cells
Antiviral response
Inflammation of central nervous system
Engulfment of cells
Degranulation of phagocytes
Recruitment of phagocytes
D
Up-regulated genes
Down-regulated genes
ARM
IRM
Trx80
277
366
83
84
107
33
24
24
4
31
62
11
350
439
NS
***
E
IRM-specific genes
Vehicle
TRX80
F
Ifit1 normalized counts (DESeq2)
Ifit2 normalized counts (DESeq2)
Ifit3 normalized counts (DESeq2)
Irf7 normalized counts (DESeq2)
Oasl2 normalized counts (DESeq2)
Isg15 normalized counts (DESeq2)
Igf1 normalized counts (DESeq2)
Spp1 normalized counts (DESeq2)
Ank normalized counts (DESeq2)
Vehicle
Trx80

565 **Figure 3. Trx80 induces an interferon type-I response in microglia**. **A)** Heatmap of differentially
566 expressed genes identified by RNA-seq (pval <0.05) between mouse primary microglia treated with
567 1 μM Trx80 for 24h and vehicle-treated controls. **B)** Volcano plot of the differential gene expression
568 analysis between microglia treated with Trx80 vs vehicle (PBS) (cutoffs: padj < 0.05; log2 fold
569 change > 1). **C)** Pathway analysis of Trx80-treated microglia versus vehicle. This analysis was
570 performed with the Ingenuity Pathway Analysis (Qiagen) on genes that were differentially
571 expressed (pval< 0.05). **D)** Venn diagram showing the overlap of downregulated (blue) and
572 upregulated (red) DEGs in Trx80-activated microglia with the gene expression signatures (up and
573 downregulated) of Activated Response Microglia (ARM, Red) and Interferon Response Microglia
574 (IRM, Yellow). Statistical analysis was performed with a Fisher's exact test (***p<0.0001). **E)**
575 Heatmap of the expression levels of all the unique gene identifiers of IRMs in control and Trx80-
576 treated microglia. **F)** Normalized counts (DESeq2) of *Ifit2, Ifit3, Irf7, Oasl2, Ifit1, Isg15, Igf1, Spp1*
577 and *Ank* genes expression in Trx80-treated microglia versus vehicle-treated microglia (*p<0.5;
578 **p<0.01).
579

580 **Figure 4**

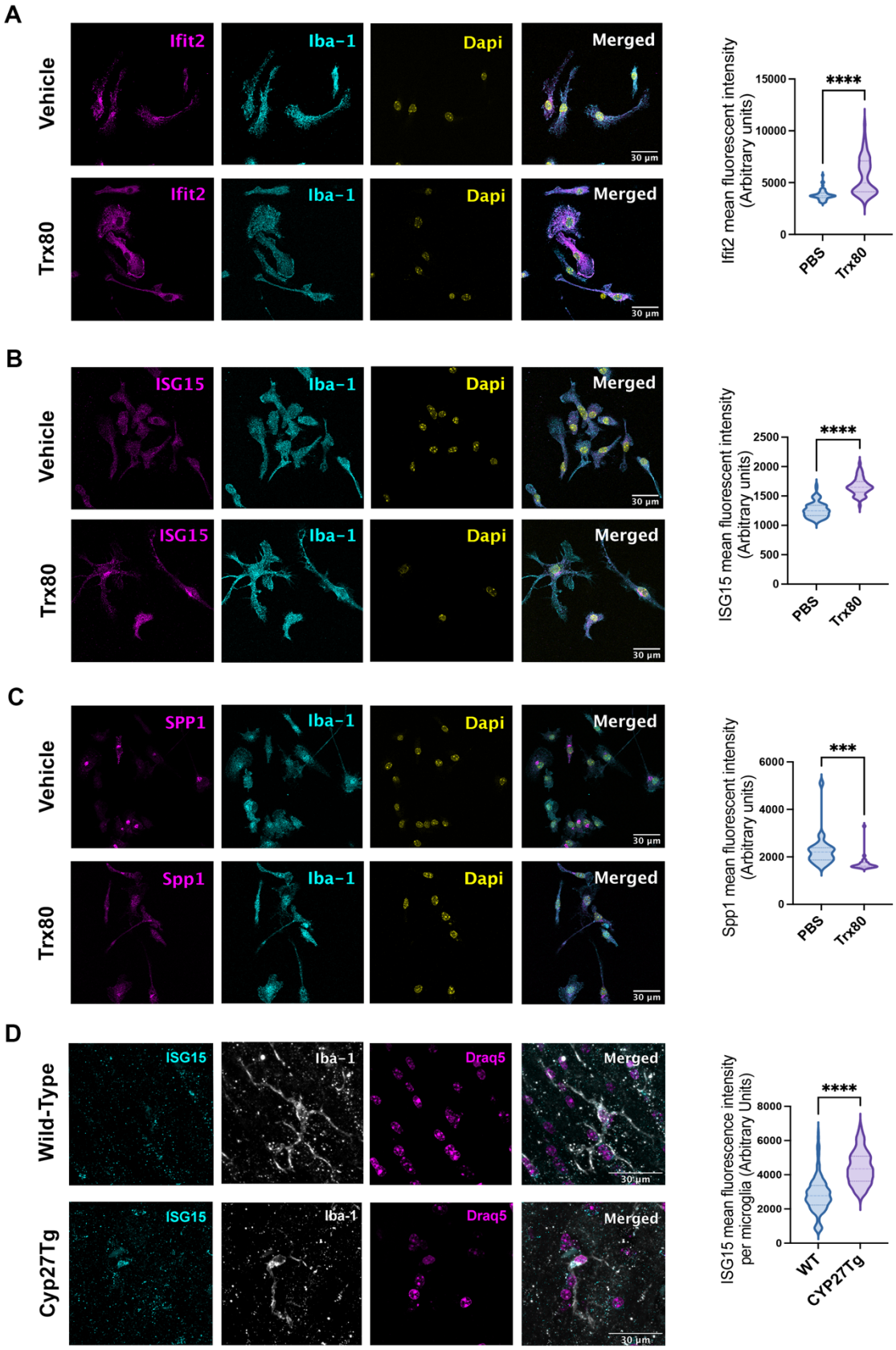
A
Vehicle
Trx80
Ifit2
Iba-1
Dapi
Merged
30 µm
Ifit2 mean fluorescent intensity (Arbitrary units)
15000
10000
5000
0
****
PBS
Trx80
B
Vehicle
Trx80
ISG15
Iba-1
Dapi
Merged
30 µm
ISG15 mean fluorescent intensity (Arbitrary units)
2500
2000
1500
1000
500
0
****
PBS
Trx80
C
Vehicle
Trx80
SPP1
Spp1
Iba-1
Dapi
Merged
30 µm
Spp1 mean fluorescent intensity (Arbitrary units)
6000
4000
2000
0
***
PBS
Trx80
D
Wild-Type
Cyp27Tg
ISG15
Iba-1
Draq5
Merged
30 µm
ISG15 mean fluorescence intensity per microglia (Arbitrary Units)
8000
6000
4000
2000
0
****
WT
CYP27Tg

581 **Figure 4. Increased Interferon related protein levels in Trx80-treated microglia. A)**
582 Immunofluorescence analysis and quantification of Ifit2 protein (magenta) in Trx80-treated (1 μM
583 Trx80 for 24h) versus vehicle-treated microglia (cyan). Nuclei are stained with DAPI (yellow). **B)**
584 Immunofluorescence analysis and quantification of ISG15 protein (magenta) in Trx80-treated
585 microglia vs vehicle treated. **C)** Immunofluorescence analysis and quantification of Spp1 protein
586 (magenta) in Trx80-treated microglia vs vehicle treated. Scale bar represents 30 microns. **D)**
587 Immunofluorescence analysis and quantification of ISG15 protein (cyan) in 22 months old Cyp27Tg
588 mice cortical microglia (grey). Nuclei are stained with Draq5 (magenta) Scale bar represents 30
589 microns. Statistical analysis was performed by Student t-test (***$p<0.001$),****$p<0.0001$).
590

591 **Figure 5**

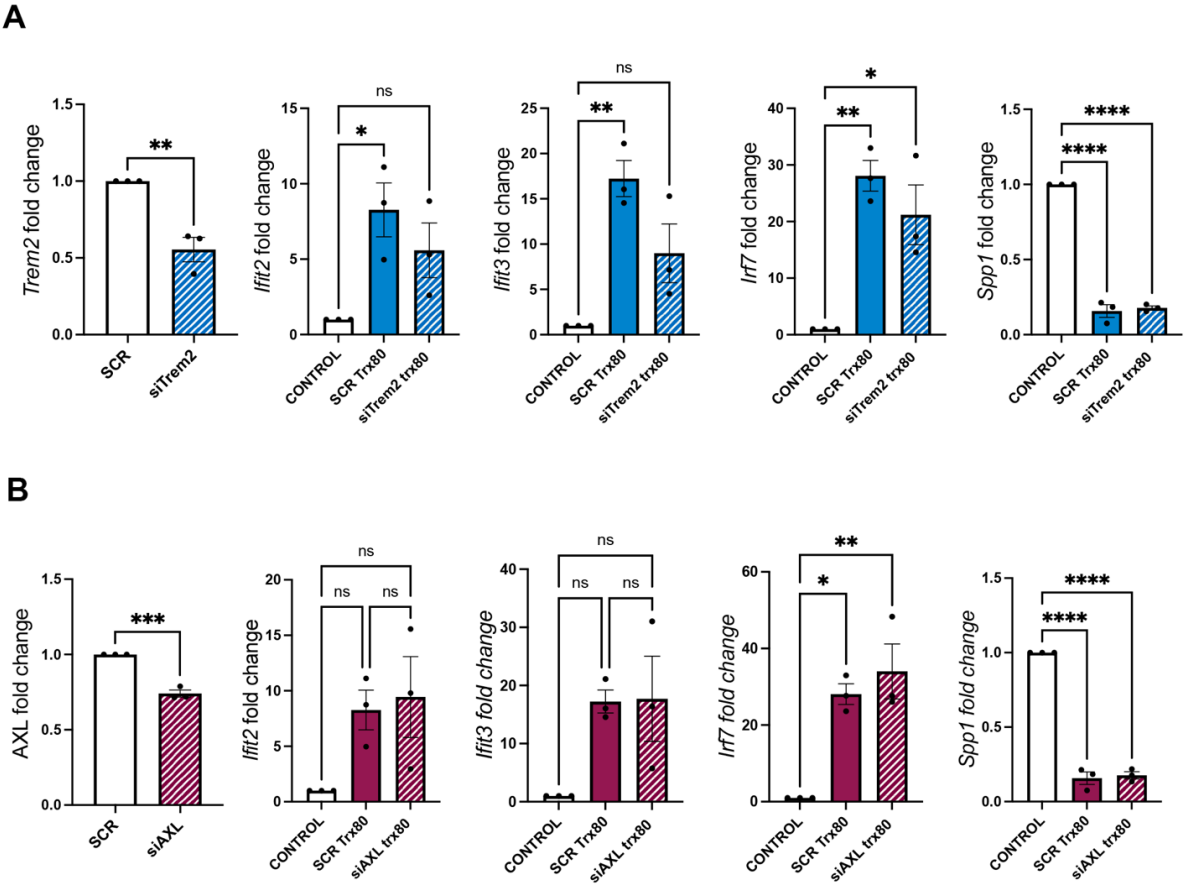

592

593 **Figure 5. Trem2 silencing attenuates interferon-related gene up-regulation in Trx80-treated**
594 **microglia. A)** *Trem2*, *Ifit2*, *Ifit3*, *Irf7* and *Spp1* gene expression fold change in SCR Trx80 microglia
595 (scrambled siRNA-transduced and Trx80-treated microglia) and siTrem2 Trx80 microglia (siTrem2
596 siRNA-transduced and Trx80-treated microglia) compared to their respective controls, that were
597 given a value of 1 (scrambled siRNA-transduced, PBS-treated microglia and siTrem2 siRNA
598 transduced, PBS treated microglia, respectively). **B)** *Axl, Ifit2*, *Ifit3*, *Irf7* and *Spp1* gene expression
599 fold change in SCR Trx80 microglia (scrambled siRNA-transduced and Trx80-treated microglia)
600 and siAxl Trx80 microglia (siAxl siRNA-transduced and Trx80-treated microglia) compared to their
601 respective controls, that were given a value of 1 (scrambled siRNA-transduced, PBS-treated
602 microglia and siAxl siRNA transduced, PBS treated microglia, respectively). Only one bar has been
603 plotted as control for simplification purposes. Statistical analysis between groups was performed
604 by one-way ANOVA (*p<0.5; **p<0.01; ****p<0.0001).
605